



# Grain-size-dependent dielectric properties in nanograin ferroelectrics

Ziming Cai<sup>1</sup>  | Xiaohui Wang<sup>1</sup> | Wei Hong<sup>2,3</sup> | Bingcheng Luo<sup>1</sup> | Qiancheng Zhao<sup>1</sup>  | Longtu Li<sup>1</sup>

<sup>1</sup>State Key Laboratory of New Ceramics and Fine Processing, School of Materials Science and Engineering, Tsinghua University, Beijing, China

<sup>2</sup>Department of Aerospace Engineering, Iowa State University, Ames, Iowa

<sup>3</sup>Global Station for Soft Matter, Global Institution for Collaborative Research and Education, Hokkaido University, Sapporo, Japan

## Correspondence

Xiaohui Wang and Longtu Li, State Key Laboratory of New Ceramics and Fine Processing, School of Materials Science and Engineering, Tsinghua University, Beijing, China.

Emails: wxh@mail.tsinghua.edu.cn and llt-dms@mail.tsinghua.edu.cn

## Funding information

National Basic Research Program of China, Grant/Award Number: 973 Program 2015CB654604; National Natural Science Foundation of China, Grant/Award Number: 51672148

## Abstract

A series of ferroelectric ceramic models with grain and grain-boundary structures of different sizes are established via Voronoi tessellations. A phase-field model is introduced to study the dielectric breakdown strength of these ferroelectric ceramics. Afterward, the relation between the electric displacement and electric field and the hysteresis loop are calculated using a finite element method based on a classical and modified hyperbolic tangent model. The results indicate that as the grain size decreases, the dielectric strength is enhanced, but the dielectric permittivity is reduced. The discharge energy density and energy storage efficiency of these ferroelectric ceramics extracted from the as-calculated hysteresis both increase along with a decrease in their grain size at their breakdown points. However, under the same applied electric field, the ferroelectric ceramic with a smaller grain size possesses a lower discharge energy density but a higher energy storage efficiency. The results suggest that ferroelectric ceramics with smaller grain sizes possess advantages for applications in energy storage devices.

## KEYWORDS

dielectric breakdown, energy storage density, grain-size effect, nanostructure

## 1 | INTRODUCTION

High-energy density, environmentally friendly, and low-cost energy storage devices are in high demand due to growing environmental problems and the rapid development of renewable energy generation.<sup>1–3</sup> Multilayer energy storage ceramic capacitors (MLESCCs) are fabricated with hundreds of thin dielectric layers arranged in parallel with alternating interlayer metal electrodes. This structure leads to a very high volumetric capacitance, and the MLESCCs are suitable for surface-mount electronics with superior mechanical and thermal properties.<sup>4</sup> Therefore, MLESCCs are considered one of the most promising candidates for energy storage devices and other applications including

hybrid electric vehicles and kinetic energy weapons.<sup>5</sup> Generally, the dielectric layers are fabricated with ferroelectric ceramics of high dielectric permittivity, such as barium titanate (BaTiO<sub>3</sub>), to achieve a high capacitance. The commercially available MLESCCs use dielectric layers with thicknesses ~1 μm or less.<sup>6,7</sup> Accordingly, the grain size of these ferroelectric ceramics should be approximately 50–150 nm to meet the temperature stability requirement and to maintain reliable performance.<sup>8,9</sup> However, the dielectric and energy storage properties are highly correlated with the grain size of these ferroelectric ceramics, which has attracted the attention of numerous researchers. In theory, the energy density ( $J$ ) of an MLESCC can be calculated by

$$J = \int_0^{D_{\max}} E dD, \quad (1)$$

where  $E$ ,  $D$ , and  $D_{\max}$  are the electric field, the electric displacement, and the maximum electric displacement at breakdown, respectively. If we assume a constant dielectric permittivity  $\epsilon$ , then

$$J = \frac{1}{2} \epsilon E^2. \quad (2)$$

It is clear that the dielectric permittivity and breakdown strength are 2 major factors that determine the energy density of the MLESCC. The grain-size-dependent dielectric permittivity of BaTiO<sub>3</sub>-related ferroelectric ceramics have been validated through a vast number of experiments.<sup>10–14</sup> Moreover, there have been some mechanism analyses of the size-dependent dielectric permittivity based on numerical modeling.<sup>15–17</sup> However, few experimental reports concerning the grain-size dependence of the dielectric breakdown strength<sup>18</sup> and even fewer mechanistic analyses have been carried out on the size-dependent dielectric breakdown of ferroelectric ceramics. It has been reported that the dielectric breakdown strength dominates the energy performance in ferroelectric materials compared to the dielectric permittivity, especially under an ultrahigh electric field from the experimental aspect.<sup>19</sup> Furthermore, the energy storage efficiency is considered one of the most important indicators of ferroelectric energy storage ceramics, which is why relaxor ferroelectric ceramics are attracting increasingly more attention in applications of energy storage devices.<sup>20–25</sup> Such energy storage densities can be easily calculated from electric hysteresis loops.

In this contribution, 4 nanostructured ferroelectric ceramics containing grain and grain-boundary structures of different grain sizes are constructed via a Voronoi tessellation. Over these structures, a phase-field method is introduced to evaluate the dielectric breakdown strength of these ferroelectric ceramics. Afterward, the relationship between the electric field displacement and applied electric field is studied using a finite element method based on a classical and modified hyperbolic tangent model. The electric hysteresis loops of these 4 ferroelectric ceramics under their breakdown electric field and a chosen electric field are calculated. The dielectric permittivity, energy density, and energy storage efficiency of these ferroelectric ceramics are also extracted from the calculated electric hysteresis loops.

## 2 | MODELING

To illustrate the grain-size effect on the dielectric and energy storage properties, 4 nanostructured ferroelectric

ceramic models with different grain sizes, containing both grain (blue domain) and grain-boundary (green domain) structures, are constructed, as shown in Figure 1. The length and height of all models are fixed at 600 and 1200 nm, respectively. The grain size of these models ranges from 50 to 125 nm, and the grain-boundary thickness is considered as grain-size independent<sup>15</sup> and taken to be approximately 5 nm. These structures can be regarded as a ferroelectric-dielectric composite, in which the grain boundaries are linear dielectric, while the grains are ferroelectric. The detailed descriptions of the phase-field models on the dielectric breakdown and the modified hyperbolic tangent model on the electric hysteresis are presented as follows.

### 2.1 | Phase-field model for the dielectric breakdown

Following Pitike and Hong,<sup>26–28</sup> a phase-field model is developed by drawing an analogy between the dielectric breakdown and mechanical fracture. To characterize the dielectric breakdown behavior of these ferroelectrics, we introduce a scalar phase field  $s(x, y, t)$ . The value of  $s$  varies from 0 to 1, which, respectively, features the fully damaged state and the intact state. The fully damaged part becomes conductive and is modeled as a dielectric of very high permittivity,  $\epsilon_{\text{ini}}/\eta$ , where  $\epsilon_{\text{ini}}$  is the initial permittivity and  $\eta$  is a small enough number, taken to be  $10^{-4}$  in the current study. For an intermediate state, the permittivity is interpolated by

$$\epsilon(s) = \frac{\epsilon_{\text{ini}}}{f(s) + \eta}, \quad (3)$$

where  $f(s) = 4s^3 - 3s^4$ . Furthermore, the ferroelectric ceramics include both grains and grain boundaries. As mentioned above, the relative permittivity of grains is electric field dependent following Johnson's approximation<sup>29</sup>:

$$\epsilon_g(E) = \frac{\epsilon_g(0)}{(1 + kE^2)^{1/3}}, \quad (4)$$

where  $\epsilon_g(0)$  is the zero-field relative permittivity and is taken to be 2000, which is typical for ferroelectric ceramics such as BaTiO<sub>3</sub>.<sup>30</sup> The parameter  $k$  is a material constant that is related to the Johnson's parameter  $\beta$  by  $k = 3\beta(\epsilon_0\epsilon_g(0))^3$  with  $\epsilon_0$ , as the vacuum permittivity. On the other hand, the relative permittivity of the grain boundary,  $\epsilon_{\text{gb}}$  is assumed to be field independent with values close to several other nonferroelectric titanates.<sup>31,32</sup> Here, we take  $\epsilon_{\text{gb}} = 100$  in our simulation.<sup>33,34</sup> Thus, the permittivity of these ferroelectric ceramics such as BaTiO<sub>3</sub> can be written as<sup>35</sup>:

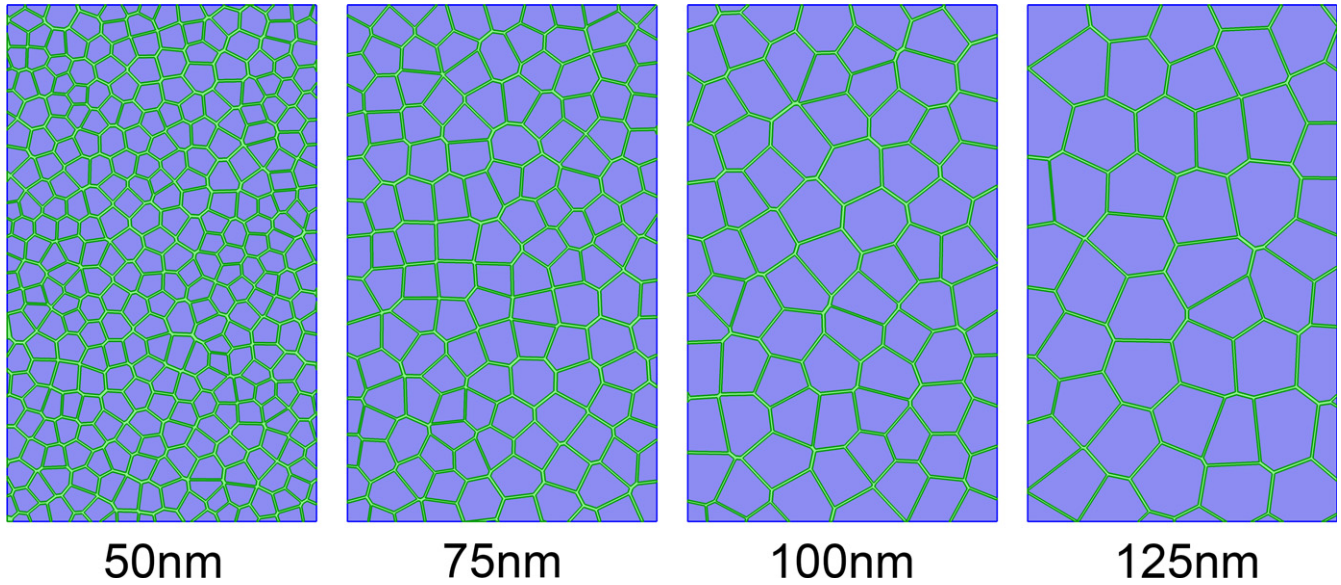


**FIGURE 1** Voronoi polygonal structured ferroelectrics containing grains of different sizes and grain boundaries of the same thickness [Color figure can be viewed at [wileyonlinelibrary.com](http://wileyonlinelibrary.com)]

$$\varepsilon_{\text{ini}}(E) = \begin{cases} \frac{\varepsilon_g(0)}{(1+kE^2)^{1/3}} & \text{in grain} \\ \varepsilon_{\text{gb}} & \text{on grain boundary} \end{cases} \quad (5)$$

In this model, the total free energy consists of complementary electrostatic energy per unit volume,

$$W_{\text{es}}(E, s) = \begin{cases} -\int_0^{E_{\text{max}}} \frac{\varepsilon_0 \varepsilon_g(s) E}{(1+kE^2)^{3/2}} dE & \text{in grain} \\ -\frac{\varepsilon_0 \varepsilon_{\text{gb}}(s)}{2} E \cdot E & \text{on grain boundary} \end{cases},$$

the energy of damage,  $W_d(s) = W_c[1 - f(s)]$ , with  $W_c$  indicating the critical density of the electrostatic energy, and the gradient energy term to regulate the sharp phase boundaries,  $W_i(\nabla s) = \frac{\Gamma}{4} \nabla s \cdot \nabla s$ . The material parameter  $\Gamma$  is approximately the breakdown energy.<sup>20</sup> Breakdown occurs if such a process decreases the total potential energy of the system

$$\Pi[s, \phi] = \int_{\Omega} [W_{\text{es}}(E, s) + W_d(s) + W_i(\nabla s)] dV. \quad (6)$$

Assuming linear kinetics:  $\partial s / \partial t = -m \delta \Pi / \delta s$ , with mobility  $m$  as a material parameter that characterizes the speed of the breakdown propagation in ferroelectric ceramics, we write the final normalized governing equations in dimensionless form as:

$$\begin{cases} \nabla \cdot \left[ \varepsilon_g(s) (1 + \bar{k} \nabla \bar{\phi} \cdot \nabla \bar{\phi})^{-1/3} \nabla \bar{\phi} \right] = 0 \\ \frac{\partial s}{\partial t} = -\frac{3\varepsilon_g'(s)}{4\bar{k}} \left( (1 + \bar{k} \nabla \bar{\phi} \cdot \nabla \bar{\phi})^{2/3} - 1 \right) + f'(s) + \frac{1}{2} \nabla^2 s \end{cases} \quad (7)$$

$$\begin{cases} \nabla \cdot [\varepsilon_{\text{gb}}(s) \nabla \bar{\phi}] = 0 \\ \frac{\partial s}{\partial t} = -\frac{\varepsilon_{\text{gb}}'(s)}{2} \nabla \bar{\phi} \cdot \nabla \bar{\phi} + f'(s) + \frac{1}{2} \nabla^2 s \end{cases} \quad (8)$$

in which the dimensionless quantities are denoted by over-bared symbols of the corresponding dimensional quantities. Generally, the breakdown energy grain boundary is considered higher than that of the grain. Therefore, in our simulation, the breakdown energy is set as  $\Gamma_g / \Gamma_{\text{gb}} = 1/10$ , and the nonlinear factor is taken as  $\bar{k} = 1E4$ . The phase-field model is calculated by implementing Equations (7) and (8) into COMSOL Multiphysics 5.3. The loading setup for the computational domain is shown in Figure 2A. An electric field concentrator is introduced to dominate the overall random defects. Limited by the computational power, all simulations are carried out in two-dimensional (2D) domains.

## 2.2 | Modified hyperbolic tangent model on the electric hysteresis

The polarization response is one of the essential characteristics that determines the dielectric performance of ferroelectric ceramics such as electric displacement, energy storage density, and efficiency.<sup>20</sup> The apparent polarization response can be easily measured experimentally. However, regarding the numerical model, the local electric field varies at different positions under an applied field due to the highly inhomogeneous microstructure of the ferroelectric ceramics. The overall dielectric properties should be obtained by taking all local properties into consideration. Therefore, a finite element method simulation is adopted in

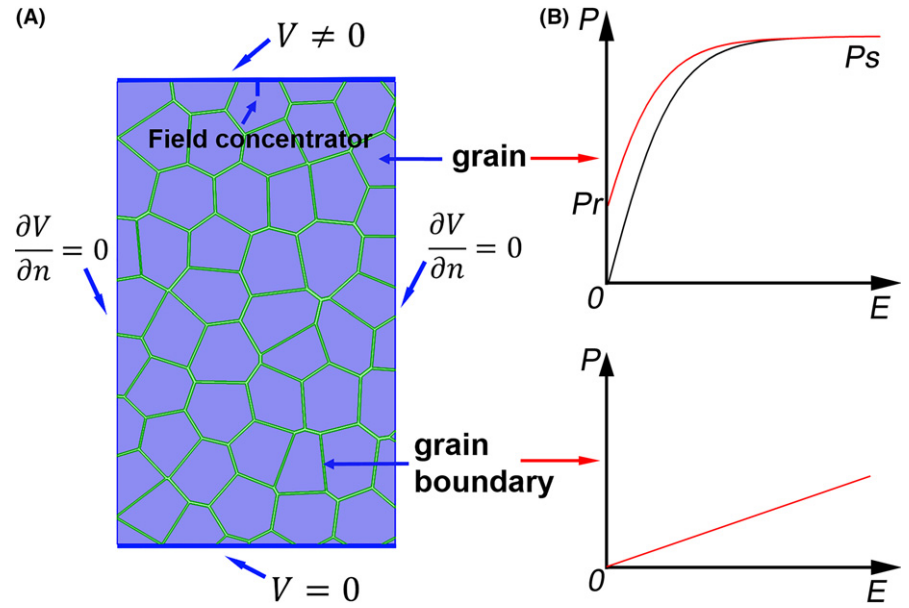


**FIGURE 2** Schematic of (A) the loading setup for the computational domain in the phase-field model and (B) the polarization response of the ferroelectric ceramic grain and grain boundary. In polarization response illustration of the ferroelectric ceramic grain. The up-branch (red curve) represents the discharging process and the down-branch (black curve) represents the charge process [Color figure can be viewed at wileyonlinelibrary.com]

our model to characterize the overall properties of these ferroelectric ceramics for their applicability in arbitrary geometries and boundary conditions.

The typical polarization response of ferroelectric ceramics under an applied electric field can be seen in Figure 2B. As mentioned in Section 2.1, the grain boundaries are considered a linear electric field response without hysteresis. The constant dielectric permittivity value of the grain boundaries is exactly the same as that described in the phase-field model. On the other hand, due to the hysteretic dielectric feature of the ferroelectric ceramic grains, as shown in the upper part of Figure 2B, the polarization response during charge and discharge processes are separately considered. A classical hyperbolic tangent function is employed during the initial charge upswing,<sup>36–38</sup> which is written as

$$P = P_s \tanh \left[ \frac{\varepsilon_0 (\varepsilon_g(0) - 1) E}{P_s} \right], \quad (9)$$

where  $P$  is the polarization under the applied field of  $E$  and  $P_s$ ,  $\varepsilon_0$ , and  $\varepsilon_g(0)$  are the saturation polarization, vacuum permittivity, and the zero-electric-field permittivity of ceramic grain, respectively. When combined with the standard constitutive definition  $D = \varepsilon_0 E + P$ , here  $D$  represents the electric displacement, and the dielectric permittivity of ceramic grain ( $\varepsilon'_c$ ) during the initial upswing can be derived by

$$\varepsilon'_c = 1 + \frac{P_s}{\varepsilon_0 E} \tanh \left[ \frac{\varepsilon_0 (\varepsilon_g(0) - 1) E}{P_s} \right]. \quad (10)$$

However, regarding the discharge downswing process, the permittivity of the ceramic grain will be different from

the one during the initial upswing due to the hysteretic character. In this case, the constitutive definition between  $D$  and  $E$  is modified to

$$D = \varepsilon_0 \hat{\varepsilon} E + P_r \quad (11)$$

where  $\hat{\varepsilon}$  is the dielectric permittivity of the ceramic grain during discharge downswing and  $P_r$  is the remnant polarization. Theoretically, if the polarization during the upswing reaches the saturation state, the polarization during the downswing is assumed by a modified hyperbolic tangent function<sup>36</sup> as

$$P = P_s \tanh \left[ \frac{\varepsilon_0 (\varepsilon_g(0) - 1) (E + E_c)}{P_s} \right], \quad (12)$$

where  $E_c$  is the magnitude of the coercive field and is linked with  $P_r$  via the relationship

$$E_c = \frac{P_s / \varepsilon_0}{(\varepsilon_g(0) - 1)} \tanh^{-1} \left( \frac{P_r}{P_s} \right). \quad (13)$$

However, in the actual case, the maximum applied electric field may not guarantee the saturation state of the polarization, which means that the achieved maximum polarization  $P_m$  will not necessarily be  $P_s$ , resulting in the remnant polarization also being less than  $P_r$ . Therefore, a modified remnant polarization  $\hat{P}_r$  is devised by Calame<sup>39</sup> in the relationship with  $P_m$ ,  $P_s$  and  $P_r$ . Simultaneously, the modified saturation polarization  $\hat{P}_s$  and coercive field  $\hat{E}_c$  can be obtained under the given values of  $P_m$  and  $P_s$ . Eventually, the dielectric permittivity of the ceramic grain during the downswing corresponds to the modified hyperbolic tangent model is written as

$$\hat{\epsilon}'_c = 1 + \frac{1}{\epsilon_0 E} \left\{ \hat{P}_s \tanh \left[ \frac{\epsilon_0 (\epsilon_g(0) - 1) (E + \hat{E}_c)}{\hat{P}_s} \right] + \hat{P}_s - P_s - \hat{P}_r \right\}. \quad (14)$$

The electric field-dependent dielectric properties, such as dielectric permittivity, electric displacement and electric field can be solved based on the Gauss' law, through

$$\nabla \cdot D = 0. \quad (15)$$

The loading setup is quite similar to that in the phase-field model shown in Figure 2A but without the field concentrator. The saturation polarization of the ceramic grain is set as 0.3 C/m<sup>2</sup>, and the remnant polarization is set to be 1/2 of the saturation polarization.<sup>30</sup>

### 3 | RESULTS AND DISCUSSION

#### 3.1 | Dielectric breakdown strength

The breakdown paths and distribution of the damage scalar (s) of these 4 nanostructured ferroelectric ceramics with different grain sizes are shown in Figure 3. We can see that the breakdown begins at the field concentrator, which is introduced to dominate the overall random defects, so that the randomness of the results can be controlled.<sup>27</sup> Afterward, the breakdown region starts to propagate across the ceramic grain and will be blocked by the nearest grain boundary since the breakdown energy of the grain boundary is much higher than that of the grain. When the applied electric field is large enough, the breakdown path will pass across the grain boundary and finally arrive at the negative electrode, which indicates that the ferroelectric ceramic is fully damaged.

During the dielectric breakdown process, the breakdown path of a smaller grain-sized ceramic will pass across more

grain boundaries and dissipate more energy, which leads to a higher breakdown strength. The largest nominal electric field during the breakdown process is then defined as the nominal breakdown strength of these ferroelectric ceramics with data plotted in Figure 4. It can be easily found that along with a decrease in the ceramic grain size, the nominal breakdown strength will be significantly enhanced. The nominal breakdown strength of the ferroelectric ceramic with a grain size of 50 nm is almost 50% higher than that a grain size of 125 nm. This finding shows good agreement with other experimental results.<sup>18,40</sup> Within the grain size scale in our simulation, the thickness of the grain boundary is considered as grain size independent, which is widely adopted by other reports.<sup>15,41</sup>

The calculated volume fractions of 50, 75, 100, and 125 nm grain-sized ferroelectric ceramics are 18.1%, 12.3%, 9.4%, and 7.4%, respectively, which directly means as the grain size decreases, the volume fraction of the grain boundaries increase gradually. The grain boundary is the “strong” part of the ceramic under an applied electric field and is difficult to damage due to its higher breakdown energy. Similarly, the ceramic grain is “weak” part and can easily be broken down compared to the grain boundary. Therefore, the enhanced dielectric breakdown strength of ferroelectric ceramics with smaller grain sizes is due to the larger amount of grain boundaries. Furthermore, the distribution of the local electric field will also affect the dielectric breakdown strength of ferroelectric ceramics, and we will specifically discuss this topic later in Section 3.2.

#### 3.2 | Dielectric response and energy storage properties

The spatial distributions of the local electric field of 4 different grain size ferroelectric ceramics under an applied electric field of 30 V/μm are shown in Figure 5A-D. It can be easily

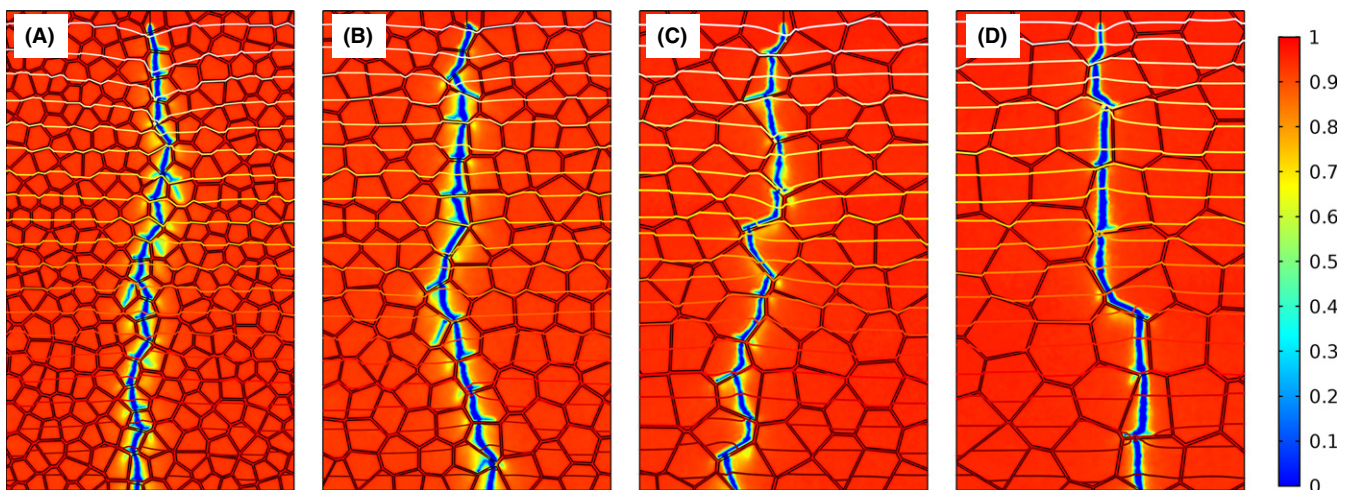


**FIGURE 3** The breakdown path featured by different grain sizes: A, 50 nm; B, 75 nm; C, 100 nm; and D, 125 nm. The contour lines are the equipotential lines of the then current electric field [Color figure can be viewed at [wileyonlinelibrary.com](http://wileyonlinelibrary.com)]

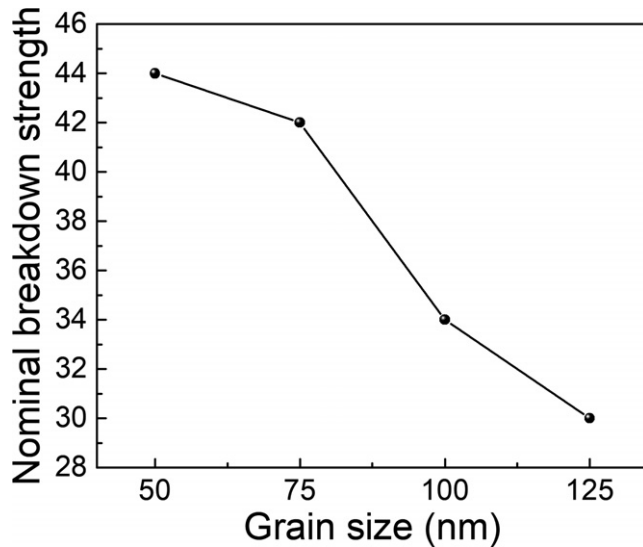


**FIGURE 4** The relationship of the nominal breakdown strength vs grain size

found that the higher electric field is stressed on the grain boundary zoom, and its value is much higher than that on the grains, which is caused by the vast dielectric permittivity difference between the ceramic grain and grain boundary according to the voltage divider rule in capacitors.<sup>42</sup> Under a given applied electric field, the distribution of the local electric field is very sensitive to the grain size. As the grain size decreases, the heterogeneity of the local electric field is weakened, which also contributes to the higher dielectric strength of the ferroelectric ceramics with smaller grain sizes. The dielectric breakdown usually occurs where the local electric field is most concentrated<sup>26</sup>; therefore, a more homogeneous distribution of the local electric field will lead to a higher dielectric breakdown strength.

A closer look at the local electric field distribution of these 4 ceramics is taken by statistically normalizing the local electric field to the applied electric field in Figure 5A-D, named the relative electric field<sup>38</sup> with the results plotted in Figure 6. The higher peak at a low relative electric field points to the grain zoom, while the lower peak points to the grain boundary zoom. Both relative electric field peaks shift toward a lower value with a decrease in the grain size, which directly indicates a more uniform local electric field distribution inside the smaller-grain-sized ferroelectric ceramic.

The dielectric breakdown strength calculated through the phase-field method in Section 3.1 is the nominal value, which is estimated by normalizing the electric and damage field. Regarding the modified hyperbolic tangent model, the unit of breakdown strength should be considered. In the opposite of normalization,<sup>28</sup> the dielectric breakdown strengths are taken as 30, 34, 42, and 44 V/ $\mu\text{m}$  corresponding to the ferroelectric ceramics with the grain size of 125, 100, 75, and 50 nm, respectively, in the modified hyperbolic tangent model. The relative electric displacement vs the applied electric field of ferroelectric ceramics with 4 different grain sizes up to their breakdown strength during upswing and downswing is shown in Figure 7A. An electric hysteresis loop is also recognized in the first quadrant, which features the hysteretic polarization response of ferroelectric ceramics under an alternating electric field. Notably, the slope of the upswing curve drops off along with the declining grain size, which indicates a decreasing dielectric permittivity. The results show good agreement with Figure 8, in which the effective dielectric permittivity calculated from the average local permittivity of these ferroelectric ceramics is displayed. One can observe that under the same applied electric field, as the grain size

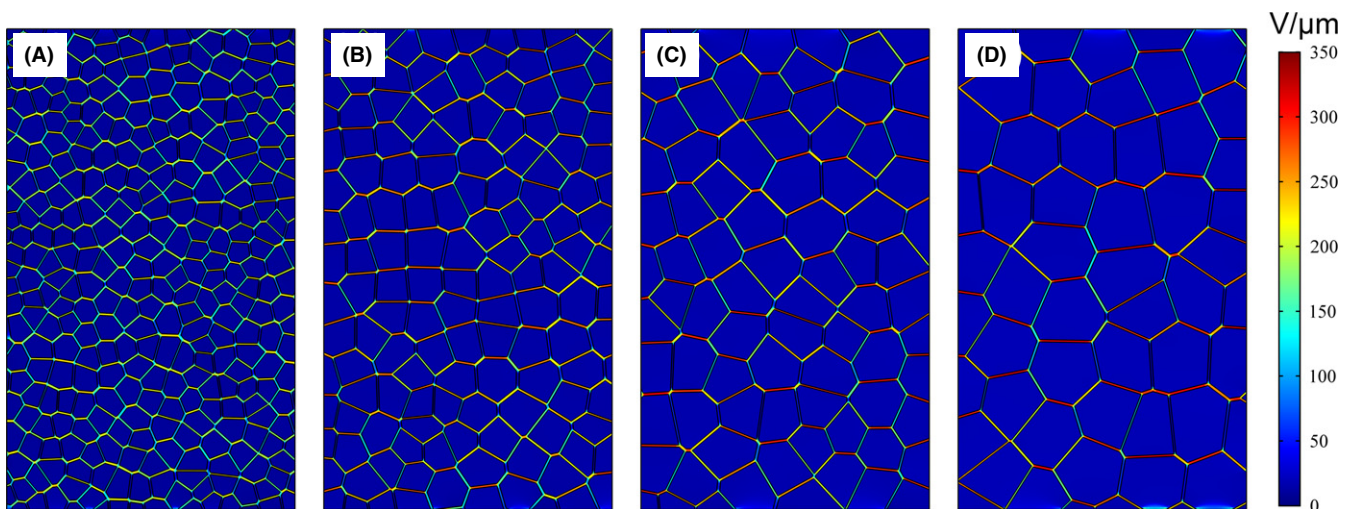


**FIGURE 5** Local electric field distribution of 4 different grain size ferroelectric ceramics: A, 50 nm; B, 75 nm; C, 100 nm; and (D) 125 nm under an applied electric field of 30 V/ $\mu\text{m}$  [Color figure can be viewed at wileyonlinelibrary.com]

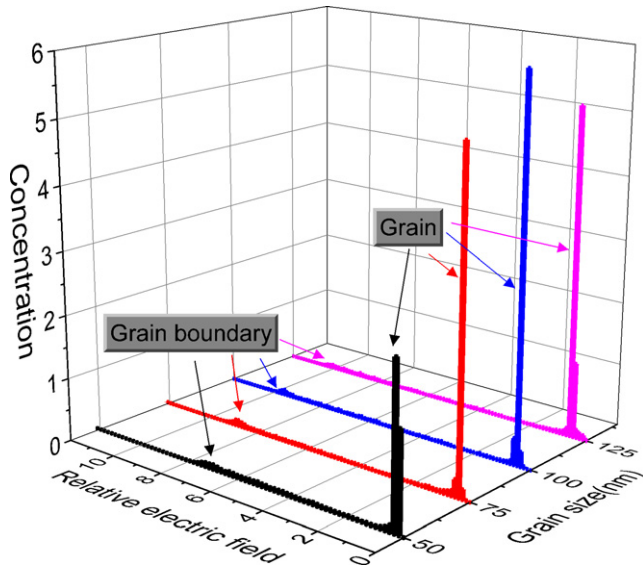


**FIGURE 6** Relative local electric field distributions of these ferroelectric ceramics at various grain sizes under a given applied electric field of 30 V/μm [Color figure can be viewed at wileyonlinelibrary.com]

decreases, the dielectric permittivity of the ferroelectric ceramic will behave the same way but with a weakened nonlinear performance.

The charge and discharge energy storage density, as well as the energy storage efficiency, can be numerically calculated from the following formulas:

$$W_{\text{cha}} = \int_0^{D_m} EdD, \quad (16)$$

$$W_{\text{dis}} = \int_{D_r}^{D_m} EdD, \quad (17)$$

$$\eta = \frac{W_{\text{cha}}}{W_{\text{dis}}} \times 100\%, \quad (18)$$

where  $D_r$  and  $D_m$  are the remnant electric displacement and maximum electric displacement, respectively, and  $W_{\text{cha}}$ ,  $W_{\text{dis}}$ , and  $\eta$  indicate the charge energy storage density, discharge energy storage density, and the energy storage efficiency, respectively.

As seen in Figure 7B, the charge and discharge energy storage densities along with the energy storage efficiencies under each of their breakdown points are calculated via Equations (16)-(18) from Figure 7A. It can be observed that although the smaller grain-sized ceramic displays lower electric displacement under the same applied electric field, it can still reach a larger discharge energy storage density than that of the larger grain-sized ceramic since it holds a higher dielectric breakdown electric field. This behavior theoretically

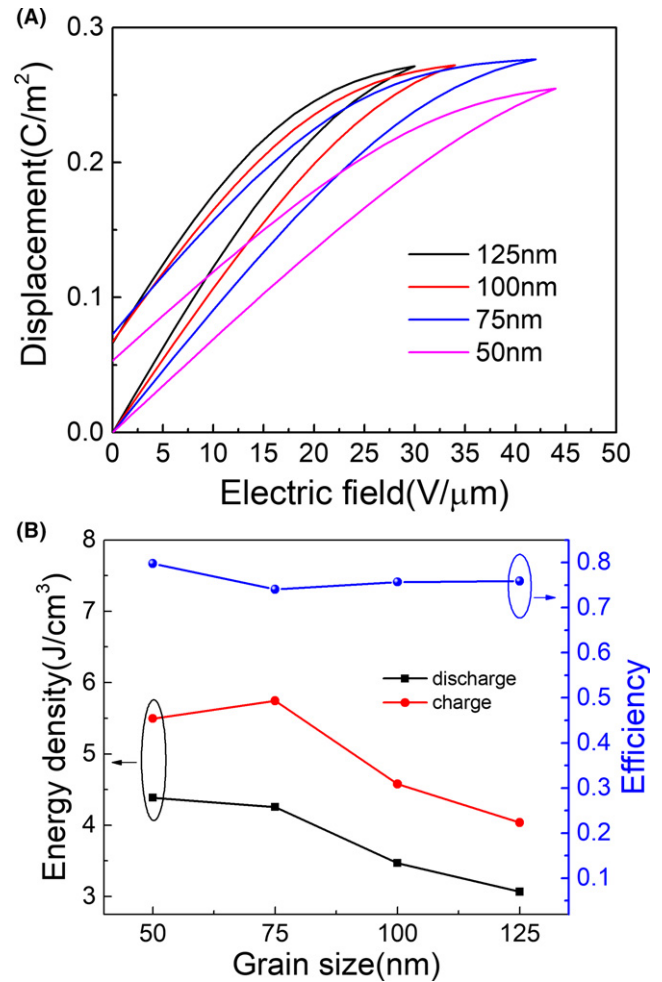


**FIGURE 7** A, Electric displacement vs. applied field of the ferroelectric ceramics with different grain sizes up to their breakdown strength. B, Energy discharge and charge density and efficiency against the grain size at each breakdown point [Color figure can be viewed at wileyonlinelibrary.com]

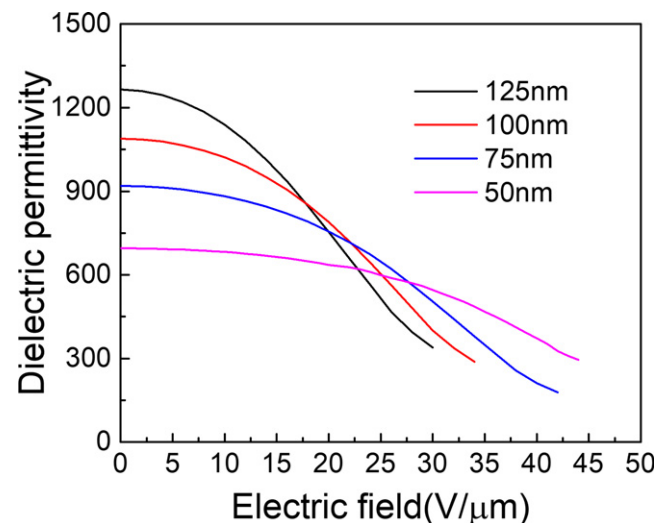


**FIGURE 8** Dielectric permittivity as a function of the electric field of the nanostructure ferroelectric ceramics with different grain sizes [Color figure can be viewed at wileyonlinelibrary.com]

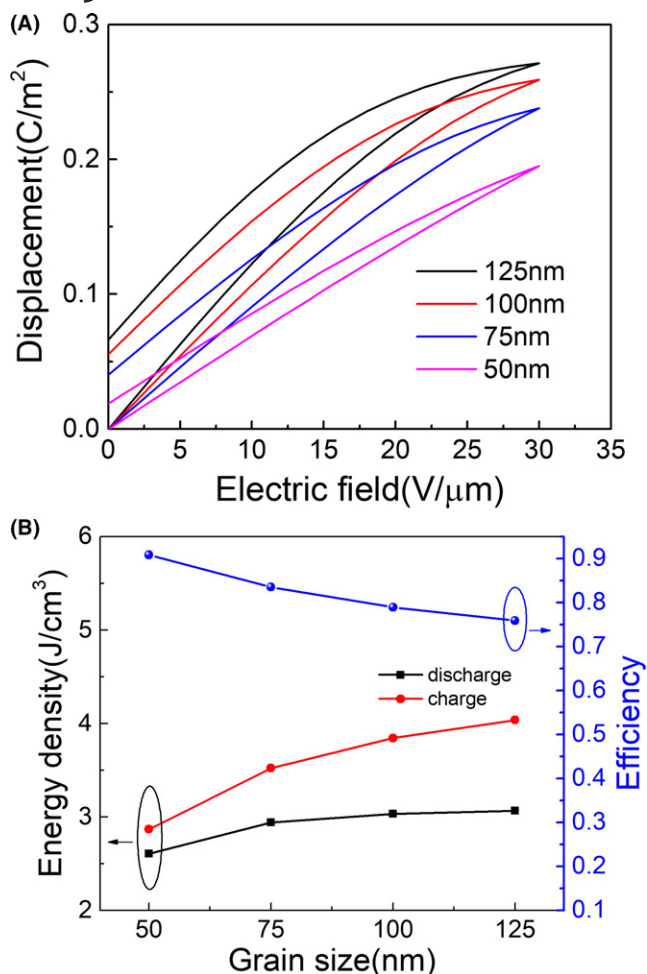


**FIGURE 9** A, Electric displacement vs applied field of ferroelectric ceramics with different grain sizes up to 30 V/μm. B, Energy discharge and charge density and efficiency against the grain size at an applied electric field of 30 V/μm [Color figure can be viewed at [wileyonlinelibrary.com](http://wileyonlinelibrary.com)]

verifies that the dielectric breakdown strength dominates the energy performance in ferroelectric ceramics. Simultaneously, the energy storage efficiency of ferroelectric ceramics with grain sizes of 50 nm is up to 80%. That is, why the ferroelectric ceramic with grain sizes of 75 nm exhibits a larger charge energy storage density but a smaller discharge energy storage density than that of a 50 nm grain-sized ceramic.

For a better comparison, the electric hysteresis loops of these 4 different grain-sized ceramics all under the same maximum applied electric field of 30 V/μm are calculated as shown in Figure 9A. Meanwhile, the calculated charge and discharge energy storage density and the energy storage efficiency under this maximum applied electric field are demonstrated in Figure 9B. It is clear that the maximum electric displacement is lower in smaller grain-sized ceramic, which results in a lower charge and discharge energy storage density. However, the remnant displacement of the small grain-sized ceramics is also reduced obviously, which leads

to a significantly enhanced energy storage efficiency of ferroelectric ceramics with small grain sizes. Such phenomenon can easily be understood through the dielectric permittivity response, as seen in Figure 8. With a decreasing grain size, the volume fraction of the grain boundary increases, as mentioned above. The dielectric permittivity inside the grain boundary is much lower than that of the grain. Thus, the effective dielectric permittivity will decline as the grain size of ceramic becomes smaller. Furthermore, the lower value of the dielectric permittivity corresponds to a lower electric displacement under the same applied field, which will lead to a lower energy storage density. However, the weakened nonlinear performance of the permittivity will improve the energy storage efficiency. In general, in spite of the lower electric displacement under the same applied electric field, ferroelectric ceramics with smaller grain sizes still show tremendous superiority in the field of energy storage, since they hold a larger dielectric breakdown strength together with a higher energy storage efficiency.

## 4 | CONCLUSION

Four nanostructured ferroelectric ceramics with different grain sizes are established via Voronoi tessellations. The dielectric breakdown strength and ferroelectric hysteresis loop are numerically calculated through a phase-field model and a finite element method based on a classical and modified hyperbolic tangent model, respectively. It is found that as the grain size decreases, the dielectric strength is enhanced, but the dielectric permittivity is reduced. Under the same applied electric field, the ferroelectric ceramic with the smaller grain size possesses a lower discharge energy density but higher energy storage efficiency. When the applied electric field reaches their own breakdown strength, the smallest grain-sized ceramic displays the largest discharge energy density and energy storage efficiency. It is highly suggested that ferroelectric ceramics with smaller grain sizes can be used for applications in energy storage devices.

## ACKNOWLEDGMENT

The work was supported by Ministry of Sciences and Technology of China through National Basic Research Program of China (973 Program 2015CB654604), National Natural Science Foundation of China (Grant No. 51672148), and also supported by CBMI Construction Co., Ltd.

## ORCID

Ziming Cai  <http://orcid.org/0000-0001-8026-023X>  
Qiancheng Zhao  <http://orcid.org/0000-0003-3134-4159>



## REFERENCES

1. Yao Z, Song Z, Hao H, Yu Z, Cao M, Zhang S, et al. Homogeneous/inhomogeneous-structured dielectrics and their energy-storage performances. *Adv Mater.* 2017;29:1601727.
2. Hao Y, Wang X, Bi K, Zhang J, Huang Y, Wu L, et al. Significantly enhanced energy storage performance promoted by ultimate sized ferroelectric BaTiO<sub>3</sub> fillers in nanocomposite films. *Nano Energy.* 2017;31:49–56.
3. Yang Z, Du H, Qu S, Hou Y, Ma H, Wang J, et al. Significantly enhanced energy storage density in transparent potassium-sodium niobate-based lead free ceramics. *J Mater Chem A.* 2016;36:13778–85.
4. Pan M-J, Randall CA. A brief introduction to ceramic capacitors. *IEEE Electr Insul Mag.* 2010;26:44–50.
5. Qu B, Du H, Yang Z, Liu Q. Large recoverable energy storage density and low sintering temperature in potassium-sodium niobate-based ceramics for multilayer pulsed power capacitors. *J Am Ceram Soc.* 2017;100:1517–26.
6. Gong H, Wang X, Zhang S, Wen H, Li L. Grain size effect on electrical and reliability characteristics of modified fine-grained BaTiO<sub>3</sub> ceramics for MLCCs. *J Eur Ceram Soc.* 2014;34:1733–9.
7. Wang X-H, Chen I-W, Deng X-Y, Wang Y-D, Li L-T. New progress in development of ferroelectric and piezoelectric nanoceramics. *J Adv Ceram.* 2015;4:1–21.
8. Tian Z, Wang X, Zhang Y, Fang J, Song T-H, Hur KH, et al. Formation of core-shell structure in ultrafine-grained BaTiO<sub>3</sub>-based ceramics through nanodopant method. *J Am Ceram Soc.* 2010;93:171–5.
9. Polotai AV, Fujii I, Shay DP, Yang G-Y, Dickey EC, Randall CA. Effect of heating rates during sintering on the electrical properties of ultra-thin Ni–BaTiO<sub>3</sub> multilayer ceramic capacitors. *J Am Ceram Soc.* 2008;91:2540–4.
10. Huan Y, Wang X, Fang J, Li L. Grain size effects on piezoelectric properties and domain structure of BaTiO<sub>3</sub> ceramics prepared by two-step sintering. *J Am Ceram Soc.* 2013;96:3369–71.
11. Hoshina T. Size effect of barium titanate: fine particles and ceramics. *J Ceram Soc Jpn.* 2013;121:156–61.
12. Zheng P, Zhang JL, Tan YQ, Wang CL. Grain-size effects on dielectric and piezoelectric properties of poled BaTiO<sub>3</sub> ceramics. *Acta Mater.* 2012;60:5022–30.
13. Sedykh P, Michel D, Charnaya EV, Haase J. Size effects in fine barium titanate particles. *Ferroelectrics.* 2010;400:135–43.
14. Wang X-H, Chen R-Z, Gui Z-L, Li L-T. The grain size effect on dielectric properties of BaTiO<sub>3</sub> based ceramics. *Mater Sci Eng, B.* 2003;99:199–202.
15. Padurariu L, Curecheriu L, Buscaglia V, Mitoseriu L. Field-dependent permittivity in nanostructured BaTiO<sub>3</sub> ceramics: modeling and experimental verification. *Phys Rev B.* 2012;85:224111.
16. Sun T, Wang X, Zhang Y, Peng B, Li L. Size effect of uniaxial stress affecting dielectric response in barium titanate. *Jpn J Appl Phys.* 2010;49:101503–4.
17. Lin S, Lü T, Jin C, Wang X. Size effect on the dielectric properties of BaTiO<sub>3</sub> nanoceramics in a modified ginsburg-landau-devonshire thermodynamic theory. *Phys Rev B.* 2006;74:134115.
18. Song Z, Liu H, Hao H, Cao M, Xu Q, Yao Z, et al. Effect of the grain boundary on the dielectric breakdown strength of (Ba<sub>0.4</sub>Sr<sub>0.6</sub>)TiO<sub>3</sub> paraelectric ceramics with various grain sizes. *2014 Joint IEEE International Symposium on the Applications of Ferroelectrics, International Workshop on Acoustic Transduction Materials and Devices & Workshop on Piezoresponse Force Microscopy (Isaf/Iwatmd/Pfm).* 2014:204–7.
19. Luo Q, Li X, Yao Z, Zhang L, Xie J, Hao H, et al. The role of dielectric permittivity in the energy storage performances of ultra-high-permittivity (Sr<sub>x</sub>Ba<sub>1-x</sub>)(Ti<sub>0.85</sub>Sn<sub>0.15</sub>)O<sub>3</sub> ceramics. *Ceram Int.* 2018;44:5304–10.
20. Li F, Zhai J, Shen B, Liu X, Zeng H. Simultaneously high-energy storage density and responsivity in quasi-hysteresis-free Mn-doped Bi<sub>0.5</sub>Na<sub>0.5</sub>TiO<sub>3</sub>-BaTiO<sub>3</sub>-(Sr<sub>0.7</sub>Bi<sub>0.2</sub>□<sub>0.1</sub>)TiO<sub>3</sub> ergodic relaxor ceramics. *Mater Res Lett.* 2018;6:345–52.
21. Cui C, Pu Y, Shi R. High-energy storage performance in lead-free (0.8-x)SrTiO<sub>3</sub>-0.2Na<sub>0.5</sub>Bi<sub>0.5</sub>TiO<sub>3</sub>-xBaTiO<sub>3</sub> relaxor ferroelectric ceramics. *J Alloys Compd.* 2018;740:1180–7.
22. Yuan Q, Yao F, Wang Y, Ma R, Wang H. Relaxor ferroelectric 0.9BaTiO<sub>3</sub>-0.1Bi(Zn<sub>0.5</sub>Zr<sub>0.5</sub>)O<sub>3</sub> ceramic capacitors with high energy density and temperature stable energy storage properties. *J Mater Chem C.* 2017;5:9552–8.
23. Yang H, Yan F, Lin Y, Wang T, Wang F, Wang Y, et al. Lead-free BaTiO<sub>3</sub>-Bi<sub>0.5</sub>Na<sub>0.5</sub>TiO<sub>3</sub>-Na<sub>0.73</sub>Bi<sub>0.09</sub>NbO<sub>3</sub> relaxor ferroelectric ceramics for high energy storage. *J Eur Ceram Soc.* 2017;37:3303–11.
24. Li W-B, Zhou D, Pang L-X. Enhanced energy storage density by inducing defect dipoles in lead free relaxor ferroelectric BaTiO<sub>3</sub>-based ceramics. *Appl Phys Lett.* 2017;110:132902.
25. Wang T, Jin L, Li C, Hu Q, Wei X. Relaxor ferroelectric BaTiO<sub>3</sub>-Bi(Mg<sub>2/3</sub>Nb<sub>1/3</sub>)O<sub>3</sub> ceramics for energy storage application. *J Am Ceram Soc.* 2015;98:559–66.
26. Cai Z, Wang X, Luo B, Hong W, Wu L, Li L. Dielectric response and breakdown behavior of polymer-ceramic nanocomposites: the effect of nanoparticle distribution. *Compos Sci Technol.* 2017;145:105–13.
27. Hong W, Pitike KC. Modeling breakdown-resistant composite dielectrics. *Procedia IUTAM.* 2015;12:73–82.
28. Pitike KC, Hong W. Phase-field model for dielectric breakdown in solids. *J Appl Phys.* 2014;115:8.
29. Johnson KM. Variation of dielectric constant with voltage in ferroelectrics and its application to parametric devices. *J Appl Phys.* 1962;33:2826–31.
30. Liu B, Wang X, Zhao Q, Li L. Improved energy storage properties of fine-crystalline BaTiO<sub>3</sub> ceramics by coating powders with Al<sub>2</sub>O<sub>3</sub> and SiO<sub>2</sub>. *J Am Ceram Soc.* 2015;98:2641–6.
31. Buscaglia MT, Viviani M, Buscaglia V, Mitoseriu L, Testino A, Nanni P, et al. High dielectric constant and frozen macroscopic polarization in dense nanocrystalline BaTiO<sub>3</sub> ceramics. *Phys Rev B.* 2006;73:064114.
32. Zhao Z, Buscaglia V, Viviani M, Buscaglia MT, Mitoseriu L, Testino A, et al. Grain-size effects on the ferroelectric behavior of dense nanocrystalline BaTiO<sub>3</sub> ceramics. *Phys Rev B.* 2004;70:024107.
33. Stamate MD. Dielectric properties of TiO<sub>2</sub> thin films deposited by a dc magnetron sputtering system. *Thin Solid Films.* 2000;372:246–9.
34. Alexandrov P, Koprinarova J, Todorov D. Dielectric properties of TiO<sub>2</sub>-films reactively sputtered from Ti in an Rf magnetron. *Vacuum.* 1996;47:1333–6.
35. Cai Z, Wang X, Luo B, Hong W, Wu L, Li L. Multiscale design of high-voltage multilayer energy-storage ceramic capacitors. *J Am Ceram Soc.* 2018;101:1607–15.

36. Miller SL, Schwank JR, Nasby RD, Rodgers MS. Modeling ferroelectric capacitor switching with asymmetric nonperiodic input signals and arbitrary initial conditions. *J Appl Phys.* 1991;70:2849–60.
37. Miller SL, Nasby RD, Schwank JR, Rodgers MS, Dressendorfer PV. Device modeling of ferroelectric capacitors. *J Appl Phys.* 1990;68:6463–71.
38. Wu L, Wang X, Li L. Enhanced energy density in core-shell ferroelectric ceramics: modeling and practical conclusions. *J Am Ceram Soc.* 2016;99:930–7.
39. Calame JP. Simulation of polarization, energy storage, and hysteresis in composite dielectrics containing nonlinear inclusions. *J Appl Phys.* 2011;110:054107.
40. Neusel C, Schneider GA. Size-dependence of the dielectric breakdown strength from nano- to millimeter scale. *J Mech Phys Solids.* 2014;63:201–13.
41. Yu S, Ning L, Weng GJ. A phase field study of frequency dependence and grain-size effects in nanocrystalline ferroelectric polycrystals. *Acta Mater.* 2015;87:293–308.
42. Bolduc L, Bouchard B, Beaulieu G. Capacitive divider substitution. *IEEE Trans Power Delivery.* 1997;12:1202–9.

**How to cite this article:** Cai Z, Wang X, Hong W, Luo B, Zhao Q, Li L. Grain-size-dependent dielectric properties in nanograin ferroelectrics. *J Am Ceram Soc.* 2018;101:5487–5496. <https://doi.org/10.1111/jace.15803>